arXiv:2412.07676v2 [cond-mat.mes-hall] 19 Dec 2024

BATIS: Bootstrapping, Autonomous Testing, and Initialization System for Quantum Dot Devices

Tyler J. Kovach,[1,*] Daniel Schug,[2] M. A. Wolfe,[1] E. R. MacQuarrie[§],[1] Patrick J. Walsh,[1] Jared Benson,[1] Mark Friesen,[1] M. A. Eriksson,[1] and Justyna P. Zwolak[3,4,5,†]

[1]*Department of Physics, University of Wisconsin-Madison, Madison, WI 53706, USA*
[2]*Department of Computer Science, University of Maryland, College Park, MD 20742, USA*
[3]*National Institute of Standards and Technology, Gaithersburg, MD 20899, USA*
[4]*Joint Center for Quantum Information and Computer Science, University of Maryland, College Park, MD 20742, USA*
[5]*Department of Physics, University of Maryland, College Park, MD 20742, USA*

(Dated: December 23, 2024)

Semiconductor quantum dot (QD) devices have become central to advancements in spin-based quantum computing. As the complexity of QD devices grows, manual tuning becomes increasingly infeasible, necessitating robust and scalable autotuning solutions. Tuning large arrays of QD qubits depends on efficient choices of automated protocols. Here, we introduce a bootstrapping, autonomous testing, and initialization system (BATIS) designed to streamline QD device evaluation and calibration. BATIS navigates high-dimensional gate voltage spaces, automating essential steps such as leakage testing and gate characterization. For forming the current channels, BATIS follows a non-standard approach that requires a single measurement regardless of the number of channels. Demonstrated at 1.3 K on a quad-QD Si/Si$_x$Ge$_{1-x}$ device, BATIS eliminates the need for deep cryogenic environments during initial device diagnostics, significantly enhancing scalability and reducing setup times. By requiring only minimal prior knowledge of the device architecture, BATIS represents a platform-agnostic solution, adaptable to various QD systems, which bridges a critical gap in QD autotuning.

I. INTRODUCTION

Quantum dot (QD) qubit devices are commonly formed by electrostatically manipulating the potential energy landscape of a two-dimensional (2D) electron or hole gas (EG or HG). This procedure produces interleaved regions of accumulated and depleted charge density that serve as QD qubits, charge sensors, and charge carrier reservoirs [1–5]. In recent years, the number of QDs in such devices has risen rapidly [6–8]. In the near term, it will no longer be possible to tune up many dots simultaneously using human-based techniques. The field of autotuning has arisen to address this challenge.

Modern semiconductor QD qubit devices have two critical features that enhance their performance, while simultaneously making autotuning challenging and essential. First, the active region of the device—the QDs, charge sensors, and reservoirs—contains no doping. All charge carriers—electrons or holes—are induced by gate voltages. No current can flow until gate voltages are applied and carriers are accumulated, yet turn-on voltages are unknown *a priori*. Furthermore, because of device drift and hysteresis, the exact voltage configuration changes not only between cooldowns but even between successive initialization steps. Second, QD device chips have multiple current channels that often serve different purposes. Some can host an array of QD qubits, while others provide a home for charge sensors. These channels are not separate until pinch-off voltages, i.e., the gate voltage threshold at which carrier accumulation is eliminated, are determined [9]. Moreover, since the accumulation and depletion of carriers must occur in alternating regions separated by only tens of nanometers, these channels must interact to enable the formation of QDs separated by tunnel barriers and proximal charge sensors.

Here, we describe a bootstrapping, autonomous testing, and initialization system (BATIS) that can automatically manipulate gate voltages to ensure that the QD chip is properly accumulated and all required pinch-off voltages are determined. BATIS takes as input the device gate layout and a high-level understanding of the desired operation, including (critically) where current channels should be continuous and which gates should divide one channel from another. The outputs of BATIS are the gate voltages that make the QD chip functional, with all current channels well delineated and all pinch-off voltages known. Importantly, in this work, the sample is kept at around 1.3 K—about 10 times warmer than other typical devices [10, 11]—which is highly desirable for high-temperature operation [12]. However, higher temperatures broaden key measurement features, such as Coulomb blockade peaks, necessitating careful fitting procedures to extract the desired parameters [13]. We show that BATIS works well at these high temperatures, which is important both for scalability and automated testing, e.g., using a cryogenic wafer prober [14, 15].

[§] Present address for ERM: Photonic, Inc. Vancouver, Canada.
[*] tkovach@wisc.edu
[†] jpzwolak@nist.gov

Previous work on autotuning has shown that correctly executed bootstrapping of QD devices sets the stage for the more specialized tuning phases. For example, setting the device topology in a modulation-doped QD device with predefined current channels has been demonstrated in Refs. [16–18]. Autotuning has similarly been implemented in an undoped SiMOS QD to achieve single-electron occupation [19]. For nanowires, which by design have a single current channel, automated tuning into fully formed QDs has been demonstrated, provided device-specific details were preconfigured [20].

Additionally, for undoped, 1D accumulation-mode QD devices, previous work has enabled progress in tuning a device topology [22, 23] and calibrating the charge state [16, 24]. Methods for automatically detecting unintentional, spurious QDs have also been proposed [25]. More recently, virtual-gate control of the electrostatic potential landscape confining holes within a 2D QD array has been demonstrated [26]. However, autonomous bootstrapping for accumulation-mode QD devices has never been attempted. Rather, most proposed tuning algorithms assumed that initial steps, such as device characterization and channel formation, have already been accomplished [27].

Our approach for BATIS differs from the existing bootstrapping algorithms, which often use efficiency as a figure of merit. By focusing on speed, such algorithms tend to be specialized to a particular device, allowing little room for benchmarking on different devices or in different experimental setups. Even if such algorithms perform well in one setting, they require a significant redesign to work in other settings. In contrast, we have specifically designed BATIS to be platform-agnostic, so that it may be applied to a variety of QD devices. While the procedural flow of BATIS is well-defined, the executable flow is automatically adjusted to suit the device architecture and external control lines, both of which are specified in the configuration file. In other words, rather than following a fixed sequence of measurements, BATIS—in real-time—chooses which steps to take and defines the expected outcomes depending on the device used. As the tuning progresses and the algorithm learns the device's characteristics, BATIS applies its knowledge to automatically customize further measurements.

Finally, we note that existing autotuning schemes focus mainly on the more advanced stages of a tune-up. These include coarse tuning, charge-state tuning, virtualization, and fine-tuning, which are sufficient for QDs formed in a preexisting channel, or when the initial bootstrapping steps are performed by hand [27]. In modern chips, hand-tuning will soon be precluded as QD processors scale up. BATIS is designed to autonomously adjust to the QD layout and perform the initial tune-up stages, including checking for fabrication defects and characterizing local and global current flow, all of which are essential for large-scale qubit implementations. It thus addresses the challenges that are about to become limiting in this widespread class of quantum semiconductor chips.

This paper is organized as follows: In Sec. II, we present an overview of BATIS, including a description of each stage of the algorithm. The experimental demonstration of BATIS is discussed in Sec. III. We conclude with a discussion of future directions in Sec. IV.

II. BATIS DESIGN

Figure 1(a) shows a gate-defined QD device that illustrates the critical features of accumulation-mode, undoped devices: multiple channels (three white arrows), regions for forming QDs (four in the qubit channel, below, and two single-QD charge sensors, above), and reservoir gates to connect these regions to ohmic contacts for current flow. This device exemplifies a commonly used fabrication strategy known as overlapping gates [28, 29].

The *screening* gates (yellow) are the closest layer of gates to the top gate oxide in the three-layer gate design and screen electric fields to prevent unwanted regions of 2DEG/2DHG, effectively isolating the channels. The second layer includes the *reservoir* (blue) and *plunger* (red) gates. The reservoirs enable the flow of electrons from the ohmic contacts toward the center of the device, where QDs will form in the electrostatic confined potential. The chemical potential of each QD is primarily controlled by the corresponding plunger gate. The final layer consists of *barrier* gates (grey), which control the tunnel couplings between QDs—both qubit QDs and charge-sensing QDs—and reservoirs. By carefully adjusting the voltages applied to each of the gates, the QD qubit chip with charge sensors is made functional [2–5].

BATIS is designed to automate the task of testing and characterizing all gates and forming all necessary 1D current channels for arbitrary-length linear QD arrays. The procedural flow of the single-button-press algorithm is depicted in Fig. 1(b).

BATIS takes as input two configuration files describing the device design and certain generic characteristics of the device and instruments. Based on that information, it performs full diagnostics and characterization of each gate and determines the proper configuration for the consecutive stage of the tuning processes. Each of the six stages in BATIS involves at least one device measurement followed by data analysis to extract characteristics of a selected subset of gates, shown in Fig. 1(b) by gray rounded rectangles. The optional *optical illumination* stage is executed on an as-needed basis. Illumination involves exposing the QD device to 780 nm light under carefully chosen gate voltages, to modify its state. Such exposure shifts the gate voltage response by modifying the amount (and if desired, the sign) of charge trapped at the semiconductor-oxide interface [21].

The algorithm follows conditional logic visually represented with arrows of different colors in Fig. 1(b). The gray arrows indicate the procedural step in the sequence. Passing the test for the current stage, marked with yellow diamonds in Fig. 1(b), initiates the next stage, as

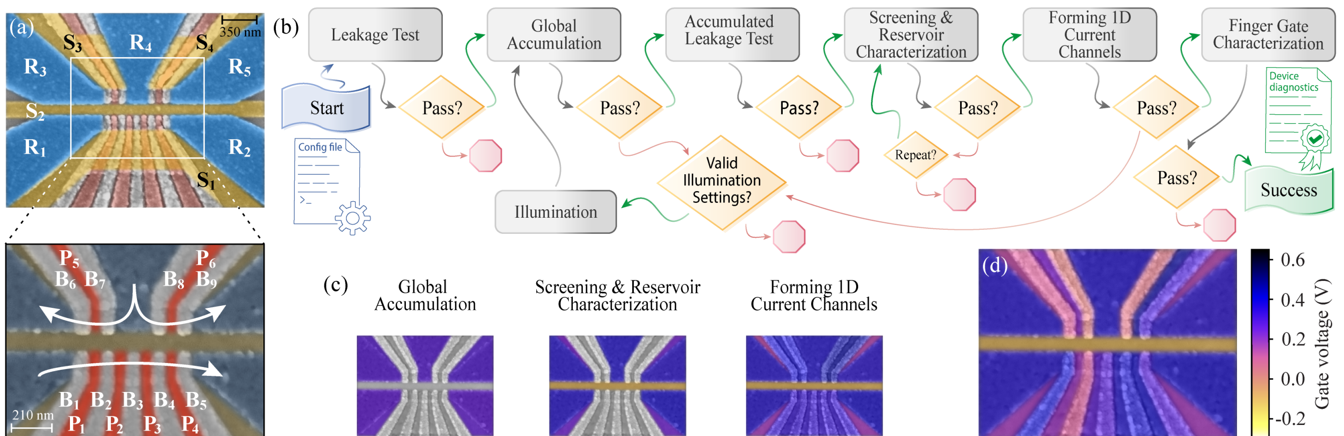

FIG. 1. (a) False-color scanning electron microscopy (SEM) image showing devices very similar to that measured here at two different magnifications. Ohmic contacts are located under the reservoir gates (R$_i$, $i = 1, \ldots, 5$; shown in blue). Screening gates (S$_i$, $i = 1, \ldots, 4$, shown in yellow) surround the three intended channels (marked with white arrows). Those channels are covered by plungers (P$_i$, $i = 1, \ldots, 6$) and barriers (B$_i$, $i = 1, \ldots, 9$). (b) The procedural flow of BATIS. The protocol starts by defining a leakage matrix to check the device leakage before (*leakage test*) and after (*accumulated leakage test*) electron accumulation. During *global accumulation*, BATIS determines the necessary gate voltage values for minimal accumulation under reservoirs and the S_1, S_3, and S_4 screening gates as determined by current flowing under those gates, see the left panel in (c). During *screening and reservoir characterization*, reservoir gate voltages are set to values above pinch-off to enable accumulation, and the screening gate voltages are set below pinch-off to ensure depletion, as shown in the middle panel in (c). When *forming 1D current channels*, the plungers and barriers accumulate carriers, and the screening gate voltages are fine-tuned as required to form the 1D channels; see the right panel in (c). Finally, all finger gate pinch-off voltages are determined during *finger gate characterization*. Beyond tuning the device, BATIS can also change the device response to gate voltages *in-situ* by illuminating with 780 nm light [21]. Active steps in autotuning are shown by gray rounded rectangles, conditional logic by yellow diamonds, and failure determinations by red stop signs. The green and red arrows indicate the passing or failing of a given step, respectively. (c) Three sample gate-voltage configurations determined by BATIS during tuning. The color value indicates the learned gate voltage, with gates not analyzed at a given stage marked in gray. The color bar applies to panels (c) and (d). (d) A false-color SEM image showing the device's final configuration as determined by BATIS. The colors indicate the gate voltage pinch-off values for the plungers and barriers, and the operating gate voltages for reservoir and screening gates.

indicated with green arrows. Failing a test can result in repeated measurements, device illumination, or termination of tuning, depending on the stage. The physical intuition behind each measurement, together with idealized and real-world data associated with each stage, are shown in Fig. 2.

Once completed, BATIS produces a device diagnostics file that stores all information about each gate learned during tuning. It also preconfigures the QD device for further use. The details of the flow of the algorithm are discussed in the following sections.

A. Initialization and First Leakage Test

The two configuration files used as input for BATIS include descriptions of all gates, desirable current channels, and the QD device connections. The files also include details about the software configuration necessary to execute BATIS and a list of variables that need to be considered at each stage. These variables consist of instrumentation limits to ensure that the algorithm does not search in ranges not supported by the instruments and device limits to protect the device from having large damaging voltages applied. Details included in configuration files allow the linking of abstract concepts about the device components with the language used in BATIS.

For example, the functionality of gates is determined automatically from the device architecture that the end user inputs, building a gate-lookup table. The files also contain a wire map and instrument information detailing the measurement system setup such that BATIS can automatically read and execute all specialized measurements, connecting the gate-lookup table with the measurement instruments. This allows BATIS to remain device- and instrument-agnostic.

BATIS starts by checking the device for leakage to the fridge ground through the oxide or any possible means in the instrumentation setup. The first leakage measurement happens before the electron accumulation during the *leakage test* stage, see Fig. 1(b). The resistances of each connection are measured with respect to each other and compiled into a *leakage matrix*, as shown in the second and third row of Fig. 2(a). The desired result is a high resistance between all the connections.

Defects during the fabrication process can result in leakage. Leakage manifests as off-colored cells in the matrix, as shown in the right panel in the second row and

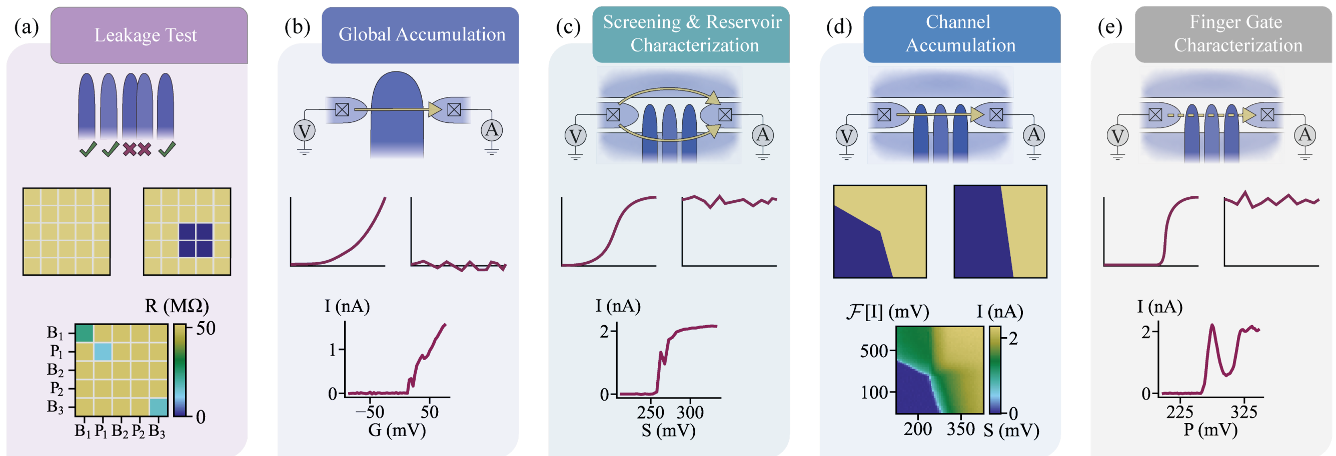

FIG. 2. BATIS measurements and example data. In (a-e), the top row explains the measurements, while the center row shows idealized cartoon representations of the key data features BATIS attempts to identify, with passing data shown on the left and failing data shown on the right. The bottom row provides an example of measurement data showing the typical imperfections against which BATIS must be robust. The arrows in the cartoons indicate the ideal current paths. (a) In the leakage test, no gate should have a low resistance to any other gate or cryostat ground (ohmic contacts are included in the test for the non-accumulated leakage test). The cartoon success data matrix shows high resistive paths on all connections. The cartoon failing matrix shows two gates shorted to each other, while the failed data matrix shows three gates shorted to ground. Devices with shorted gates are unusable. (b) For global turn-on, a rise in the current above zero as the gate voltages are increased is expected. The failure cartoon plot shows a failure to turn on. A successful turn-on is observed in the experimental data. (c) A drop in the current to the noise floor as the gate voltage is lowered is desired for pinch-off. The failure cartoon demonstrates a failure of the screening or reservoir gate to pinch off. BATIS is tolerant to small oscillations due to, e.g., accidental Coulomb blockade during pinch-off visible in the experimental data. (d) For channel accumulation, rather than relying on measuring pairs of screening gates, BATIS sweeps a single screening gate (S) against all the finger gates corresponding to that current channel, ($\mathcal{F}$). The cartoon failure measurement indicates that finger gates are too far below the threshold to be useful. As shown in the example data, the analysis must be robust to the internal structure in the region where current flows. (e) Each plunger and barrier gate must pinch off individually. The failure demonstrates a failure of the finger gate to pinch off. BATIS must tolerate Coulomb blockade oscillations which are often observed prominently during pinch-off at this tuning stage.

in the third row of Fig. 2(a). Should leakage be detected, BATIS terminates and flags the device as unusable.

B. Global Accumulation

For accumulation mode QD devices no 2DEG is present at zero applied gate voltage. Applying a non-zero bias lowers the conduction band minimum below the Fermi level, accumulating a 2DEG in the quantum well near the Si/Si_xGe_{1-x} interface. The goal of the *global accumulation* stage, see Fig. 1(b), is to determine the characteristic voltage $V_\mathcal{P}$ where enough of the 2DEG is accumulated that a significant amount of current begins to flow between the ohmic contacts, effectively turning the device on.

Determining the turn-on voltages $V_\mathcal{P}$ relies on fitting to a phenomenological function that mimics the expected behavior of the signal. Prior to fitting, the raw data is preprocessed to clean the signal. The preprocessing involves cropping the data to avoid non-linearities at the extreme limits of the data acquisition electronics followed by smoothing the data to remove noise from the signal. The processed signal is then fit to a function of the form

$$f_\delta(x) = \left[1 + \exp\left(-\frac{x - x_0}{\delta}\right)\right]^{-1}, \qquad (1)$$

where x_0 is the center of the signal and $1/4\delta$ describes the slope at x_0. The final turn-on voltage is defined as

$$V_\mathcal{P} = x_0 + 8v\,\delta, \qquad (2)$$

where $v = -0.5$ is a fixed constant specifying how much the gate needs to be adjusted to turn-on in the units of δ [30]. In addition, the saturation of the curve x_1 is defined following Eq. (2), with $v = 0.5$. In cases where the saturation of the curve is not captured in the measurement, the last point along the sweep axis becomes x_1. The first estimation of the maximum allowed voltage applied to each gate is defined as $V_{max} = (x_1 + x_{max})/2$.

Idealized successful and failing measurements for this stage are visualized in the left and right panels in the middle row of Fig. 2(b), respectively. The turn-on process in real QD devices is not always straightforward, as even a good QD device might not turn on properly when first tested. If the algorithm encounters a problem within global turn-on, it has a recovery pathway through optional *illumination*, see Fig. 1(b).

Illumination is initiated when the device fails to turn on or the turn-on voltage is much too high to be usable. After illumination, the global accumulation stage is re-initiated. If the preference is not to use illumination, BATIS allows skipping this step and going straight to repeating the global turn-on stage. Whether or not illumination should be used is an option that is pre-defined in the configuration file.

C. Accumulated Leakage Test

Once the 2DEG is accumulated, the *accumulated leakage test* is initiated. This step proceeds analogously to the first leakage check, except that it does not include the ohmic connections. This is because this leakage check is taken when the device is accumulated, and the ohmics are intentionally shorted to each other. If this stage fails, it indicates that a gate is shorted to the 2DEG flowing beneath it, which is an unrecoverable fabrication defect. Should that occur, BATIS terminates.

D. Screening and Reservoir Characterization

The global accumulation voltage does not provide gate-specific information. To learn that information, BATIS performs a series of individual gate characterizations. The first of these is performed at the *screening and reservoir characterization* stage in Fig. 1(b).

With the 2DEG globally accumulated using the voltages selected from Sec. II B, BATIS depletes the voltages on individual gates until the current on the corresponding channel is pinched off, as displayed in the left panel in the second row in Fig. 2(c). BATIS uses these pinch-off curves to determine the operational configuration for reservoir gates that ensures proper 2DEG accumulation and establishes bounds for operating the screening gates.

The signals for screening and reservoir gates are pre-processed as described in Sec. II B. Once cleaned, the derivative of the current vs. voltage signal, dI/dV, is fit to the derivative of the phenomenological function given in Eq. (1). The pinch-off, guaranteed isolation, and operating voltages are defined following Eq. (2), with $v = -0.5$, $v = -1.0$, and $v = 0.5$, respectively. The operating voltage for the central screening gate is handled separately as it has to satisfy two constraints: ensuring that all current channels can be formed without merging. By default, $v = -0.75$. If at the subsequent state, a failure to form 1D current channels is observed twice, BATIS adjusts this parameter in increments defined as $v_\tau = (-1)^p\, 0.02$, where $p = \{0, 1\}$ is chosen at random.

The typical failure edge cases for this stage include too much depletion and too much accumulation; see the second row, the right column of Fig. 2(c). If the channel below a gate is extraordinarily depleted, no voltage can be applied to the gate to accumulate it. On the other hand, if the channel is too accumulated, it is not possible to pinch it off. However, both types of issues would have been detected at the global accumulation stage, prompting the initiation of device illumination. Thus, the no change in current at this stage has to be caused either by an issue with the instrument or a broken gate. To check whether this is the case, the algorithm executes a repeated measurement. If the error is observed a second time, it indicates an issue with the gate and the algorithm terminates.

E. Forming 1D Current Channels

The 1D current channels are formed by selectively removing 2DEG from certain regions of the device. It requires depleting the screening gates and accumulating the plungers and barriers (often collectively called *finger gates*) such that the current flows between the screening gates along the desirable path, as seen in the top row of Fig. 2(d).

Determining voltages where 1D channels are properly formed is typically done by sweeping two screening gates simultaneously in a 2D sweep while holding the finger gates constant. The formation of the channel manifests as a triangular-sloped region (the so-called *triangle plots*) [31]. If the finger gates are not accumulated enough, this region will not form. Thus, multiple scans with incremented finger gate voltages—a three-dimensional dataset—are often required before the region is observed for all required channels.

BATIS employs a different approach to simultaneously accumulate multiple 1D channels using only a single two-dimensional dataset. Instead of sweeping two screening gates, BATIS takes a 2D voltage scan while sweeping one screening gate against all of the finger gates between that gate and the other screening gate used to form the 1D channel (typically the central screening gate). BATIS uses the channel isolation ($\mathrm{V}_{\mathcal{I}}$) and the operating points ($\mathrm{V}_{\mathcal{O}}$) to prepare the device for characterizing the remaining screening gates by sweeping from $\mathrm{V}_{\mathcal{I}}$ past $\mathrm{V}_{\mathcal{P}}$. The 1D channel formation technique implemented in BATIS requires a single measurement for each pair of gates, which makes it much more efficient than the standard approaches.

The plot in the left panel in the second row Fig. 2(d) exhibits three characteristic regions: a no-current region in the bottom left, a screening-gate-dominated region in the bottom right, and a finger-gate-dominated region in the top left. BATIS automatically selects an operating point in the top left part of the plot, near the boundary between the current and the no-current regions. The automatic analysis of the regions and their respective boundaries is enabled by fitting a synthetic model to the experimental data, similar to Ref. [32]. Additional criteria based on the local properties, e.g., estimated resistance and derivatives of the measurement, are used to optimize the selection of the final point $\mathrm{V}_{\mathcal{O}}^{I_\ell}$ for $\ell = 1, 2, 3$, among numerous candidates in the operating region.

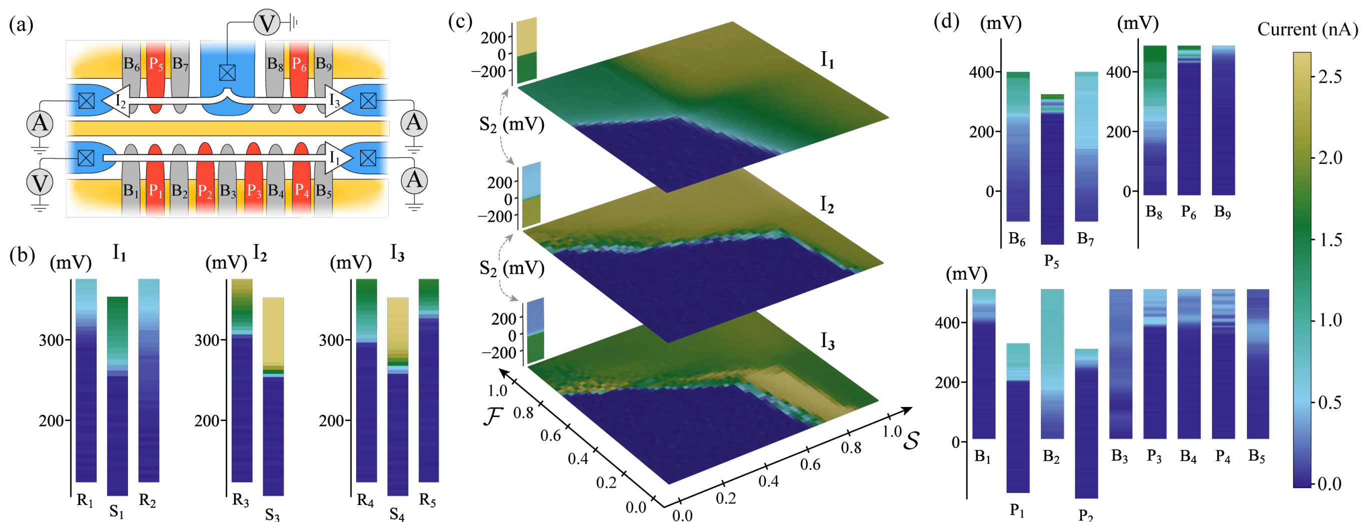

FIG. 3. Successful BATIS tune-up on a three-channel, six-QD device. (a) A schematic circuit diagram of the QD device shown in Fig. 1(a) depicting how BATIS understands the device. Numbered current paths are shown, as are the source voltage and current amplifier connections to ohmic contacts. This information is entered into the configuration file. (b) Pinch-off data for all reservoir gates and external screening gates grouped by measurement channel. The acquired signal for gate S_1 extends over twice the voltage range of all other measurements. However, as the low-voltage data away from the transition region exhibit no strong features, the plotted voltage range is truncated for visualization purposes. (c) The results of the channel accumulation measurements for each current channel. The $\mathcal{F}$ axis represents the normalized voltage range applied to all of the finger gates, and the $\mathcal{S}$ axis is the normalized voltage range applied to the screening gates bordering a given channel. The finger gates for channel I_1 in panel (a) are swept from −104 mV to 724 mV, the finger gates for channel I_2 in panel (a) are swept from −91 mV to 727 mV, and the finger gates for channel I_3 are swept from −83 mV to 729 mV. The screening gates are swept from 127 mV to 427 mV, and −18 mV to 282 mV, and from 50 mV to 350 mV for channels I_1, I_2, I_3, respectively. The S_2 pinch-off curves are included for each channel. (d) Pinch-off data for all finger gates. BATIS has adjusted the trapped charge under the gates by means of biased illumination, so that all pinch-off voltages occur in a reasonable range, in this case between −200 mV and 500 mV. The color bar on the right corresponds to all plots in (b), (c), and (d).

If the finger-gate-dominated region does not form, as shown in the right panel in the second row of Fig. 2(d), BATIS illuminates the device with the finger gates voltages set to be more negative than the most recent illumination. This adjustment can be found in the configuration file, we used 400 mV. After such an illumination, the entire device response can change, because of cross-talk and the interdependence of the current paths. Thus, BATIS resumes autotuning from the global accumulation step.

F. Finger Gate Characterization

Once isolated current channels are formed, finger gate pinch-offs ($V_{\mathcal{P}}$) can be measured. Ideally, as the voltage on a given finger gate is lowered, the pinch-off curves should exhibit a smooth, sigmoidal trend consistent with Eq. 1, eventually cutting off the current in the respective channels following Eq. (2) with $v = -0.5$. An idealized representation of such a curve is visualized in the left panel in the second row in Fig. 2(e).

The bottom panel in the third row of Fig. 2(e) shows a typical curve for these measurements. As the voltage is reduced, the curve begins to exhibit the characteristic Coulomb blockade oscillations typical of QD devices [13]. In principle, such oscillations could complicate any fit-based analysis. Instead, BATIS uses thresholding and slope detection to determine the pinch-off voltage on a point-by-point basis, going in the direction of increasing voltage (the reverse of how the signal was measured) to evade the small deviations of background noise, whilst capturing the first significant turn-on.

III. EXPERIMENTAL DEMONSTRATION

We now demonstrate BATIS on a 1D quadruple Si/Si_xGe_{1-x} QD device, nominally identical to the one shown in Fig. 1(a) with 24 gates. The first layer of gates is made up of four screening gates, S_i for $i = 1, \cdots, 4$, shown in Fig. 1(a) in yellow. The next layer consists of five reservoirs, R_i for $i = 1, \cdots, 5$, and six plunger gates, P_i for $i = 1, \cdots, 6$. The reservoirs are shown in Fig. 1(a) in blue, while the plungers are shown in red. The final layer consists of nine barrier gates, B_i for $i = 1, \cdots, 9$, shown in Fig. 1(a) in gray.

The goal of BATIS is to form three current channels in the quad-QD device as it learned from the gate layout in the configuration, as indicated with white arrows in

TABLE I. The summary of the four global accumulation runs. The first column indicates the channel and the derived voltages are indicated in the second column. The $V_{\mathcal{P}}$ indicates the detected turn-on while V_{max} is the maximum accumulation voltage for a given channel. BATIS chose to initiate illumination after the first three runs. The fourth run was satisfactory and the algorithm proceeded to the next stage.

	Voltages	Run 1	Run 2	Run 3	Run 4
I_1	$V_{\mathcal{P}}$ (mV)	28.0	26.1	24.7	296.0
	V_{max} (mV)	81.7	78.6	75.5	349.4
I_2	$V_{\mathcal{P}}$ (mV)	28.2	20.8	23.5	308.7
	V_{max} (mV)	53.6	47.3	47.3	339.2
I_3	$V_{\mathcal{P}}$ (mV)	7.4	9.5	2.6	317.1
	V_{max} (mV)	53.6	53.6	50.4	349.4

Fig. 3(a). BATIS brings a grounded but not characterized device from Fig. 1(a) to a fully operational device in Fig. 1(d). In what follows, we explain how BATIS navigates the execution of the quad-QD device bootstrapping, testing, and characterizations.

First Leakage Test. BATIS begins by performing a device leakage test. For the quad-QD device used in our demonstration, the sample mount holding it contains 40 connections, of which 29 are used for instrument channels to control individual gates and ohmics and an additional 11 wired channels are unused for this device. Thus, the size of the leakage matrix is 40×40 to examine all possible leakage states. BATIS first checks the 40 diagonal elements of the leakage matrix. If the resistance of every connection exceeds 25MΩ, BATIS declares that there is no leakage in the device.

If any of the diagonal elements falls below the 25MΩ threshold, the device is declared leaking. Depending on where the current leak occurs, it is sometimes possible to recover a leaking device. Thus, rather than terminating, BATIS continues to fill in the leakage matrix for diagnostic purposes. Due to the symmetry of the measurements, the leakage matrix is also symmetric and only the lower triangular part of the matrix needs to be completed. Moreover, passing the threshold test by a diagonal component automatically guarantees that the entire column corresponding to that component also passes the test. Thus, only the columns corresponding to the elements below 25MΩ need to be determined. BATIS continues to fill the leakage matrix one column at a time. In the worst case, a total of 820 resistance measurements are necessary to complete the leakage matrix.

The leakage test needs to be executed only once per cooldown if under fully automatic control. This is because BATIS has built-in safety checks during voltage choice selection to avoid exceeding safe voltage breakdowns between neighboring gates for all measurements.

Global Accumulation. Next, BATIS performs the global accumulation stage. In our demonstration, the algorithm executed three rounds of illumination before the observed global turn-on values were determined to be satisfactory, occurring between 200 mV and 400 mV. By design, all gates are grounded during the first two illuminations. The first illumination is intended to completely reset the device while the second is to verify that all instruments work as intended. Because BATIS still did not find the gates in the desired range, it chose to apply voltages to all screening and reservoir gates for the third illumination. The voltages required to achieve turn-ons at around 300 mV, calculated following the protocol in Ref. [21], were set to 280 mV for gates associated with channel I_1 and I_2, and 300 mV for gates associated with channel I_3. The central screening gate, S_2, was left grounded during the illumination.

The fourth iteration of global turn-on measurement was successful. The summary of all four runs is presented in Table I. The resulting configuration of the QD device is shown in the left panel in Fig. 1(c), where the pinch-offs on all the screening gates, excluding S_2, and all of the reservoir gates are colored based on the learned gate voltage.

Accumulated Leakage Test. With the global accumulation confirmed, BATIS proceeds to the accumulated leakage test. A second leakage matrix is measured, following the same procedure as during the first leakage test. Like previously, BATIS finds that all resistances exceed 25 MΩ. Since the ohmic connections are excluded, the resulting matrix has five fewer indexes. As none of the connections leaked, only 35 measurements following the matrix diagonal were taken.

Screening and Reservoir Characterization. The next stage in BATIS involves the characterization of the screening and reservoir gates. The results of these characterizations for all tested gates are presented in Fig. 3(b). Unlike the other screening and reservoir gates, S_2 needs to be measured simultaneously on channels I_1, I_2, and I_3 since it borders all of the current channels. Because of this, the data for the S_2 pinch-off can be found in Fig. 3(c) as it needs to be organized by channel.

The voltage values are quite consistent between the sets of reservoir and screening gates intended to form the desired current channels, a feature from the illumination from earlier [21]. We note that for gate S_1, BATIS acquired the signal over a 600 mV range, i.e., twice as long as compared to all other screening gates. This is likely due to poor fit scoring using the reduced voltage scan range, which caused BATIS to perform additional measurements with an increased sweep range to be more confident in the derived pinch-off value. Since the long tail of the signal has no features, the signal shown in Fig. 3(b) is truncated to be consistent with the remaining measurements for visualization purposes.

The summary of the pinch-off voltages and the operating points selected by BATIS is presented in Table II. A device in this configuration prepared for the channel accumulation stage is shown in Fig. 1(c).

TABLE II. The summary of the derived voltages for screening and reservoir gates as determined during their characterization stage, as identified by BATIS. The first column indicates the gate. The pinch-off voltages, $V_{\mathcal{P}}$, the guaranteed isolation voltages for screening gates, $V_{\mathcal{I}}$, and the operating points for reservoirs, $V_{\mathcal{O}}$, are presented in the next three columns respectively. The gates are organized top down in the order they were measured.

Gate	$V_{\mathcal{P}}$ (mV)	$V_{\mathcal{I}}$ (mV)	$V_{\mathcal{O}}$ (mV)
S_2	−54.3	−176.2	−103.0
S_1	275.6	107.5	...
R_1	291.2	...	382.2
R_2	273.4	...	390.7
S_3	252.4	192.5	...
R_3	288.1	...	382.5
R_4	273.9	...	384.1
S_4	269.6	180.8	...
R_4	278.1	...	379.3
R_5	314.2	...	370.1

Forming 1D Current Channels. With all screening and reservoir gates characterized, BATIS proceeds to form the 1D current channels. The quad-QD device requires three current channels to be formed, as indicated with the white arrows in Fig. 3(a). BATIS identified three different operating points, one for each 1D current channel calculated from the simultaneous channel accumulation in Fig. 3(c). The summary of the screening and finger gates configuration for each operating point is presented in Table III, and a collapsed zero cross-talk visualization is pictured in the right panel in Fig. 1(c). The three points are consolidated into one where the voltage color for each gate is the $V_{\mathcal{O}}$ indexed by the channel the gate belongs to.

As we discuss in Sec.II E, the algorithm for 1D current channel formation implemented in BATIS does not follow the typical, triangle-plot-based strategy. Rather, it sweeps each of the three outer screening gates, i.e., S_1, S_3, and S_4, against all finger gates relevant to the given 1D current channel. The traditional triangle plots [31, 32] are orthogonal to the measured planes shown in Fig. 3(c) and would have been measurements with the S_2 axis instead. In other words, the triangle plots and the plots utilized in BATIS contain similar information on different plane cuts through the same space.

The accumulation plots in Fig. 3(c) reveal a dip in the current exiting I_3 when the current starts to flow in I_2, shown by the dark green shape imposed on top of the signal in I_3. This is due to a coupling between those two channels resulting from a shared ohmic connection to source the currents. Such a dip in the charge sensor readout is often called a *shadow*. Shadows increase the difficulty of detecting and forming isolated current channels. The accumulation plot for I_1 is much less correlated with the current flow in the two charge sensor channels,

TABLE III. The screening and finger gate configuration summary for the three operating points identified by BATIS. The first column indicates the gate(s). Columns two through four provide the screening and finger gates operational configuration, $V_{\mathcal{O}}^{I_\ell}$ with $\ell = 1, 2, 3$, for each of the operating points identified by BATIS to form channels I_1, I_2, and I_3, respectively. The finger gates are grouped based on the channel they belong to as $\mathcal{F}[I_1]$, $\mathcal{F}[I_2]$, and $\mathcal{F}[I_3]$.

Gate(s)	$V_{\mathcal{O}}^{I_1}$ (mV)	$V_{\mathcal{O}}^{I_2}$ (mV)	$V_{\mathcal{O}}^{I_3}$ (mV)
S_1	189.2	276.8	228.8
$\mathcal{F}[I_1]$	356.6	364.3	369.5
S_3	42.4	131.7	84.4
$\mathcal{F}[I_2]$	389.8	397.0	401.9
S_4	109.6	199.6	153.3
$\mathcal{F}[I_3]$	456.0	462.5	466.9

but there is still some cross-talk. This is due to separation with the S_2 gate which divides the 2DEG between the upper readout channels and the lower dot channel.

Finger Gate Characterization. The last stage of BATIS involves finger gate characterization. This characterization is done individually for all of the finger gates on the QD device. The voltage range for each measurement is always the same and predefined in the configuration file. However, due to the Coulomb blockade oscillations, the automated search for the starting voltage for some gates is more challenging than for others. This can be seen in the raw data pictured in Fig. 3(d). The resulting pinch-off values of all of these varying curves for all finger gates are presented in Table IV. This configuration is used in the final colorized SEM for the ending state of the algorithm shown in Fig. 1(d).

TABLE IV. The resulting pinch-off values, as determined by BATIS, for all the finger gates. Each of the main three columns consists of two sub-columns, and each main column associates with a set of finger gates belonging to a particular current channel on the device $\mathcal{F}[I_\ell]$, with $\ell = 1, 2, 3$. The left sub-column is a particular finger gate belonging to the selected subset of gates, and the right sub-column is the determined pinch-off voltage $V_{\mathcal{P}}$ for the finger gate.

$\mathcal{F}[I_1]$		$\mathcal{F}[I_2]$		$\mathcal{F}[I_3]$	
Gate	$V_{\mathcal{P}}$ (mV)	Gate	$V_{\mathcal{P}}$ (mV)	Gate	$V_{\mathcal{P}}$ (mV)
B_1	406.1	B_6	84.0	B_8	32.2
P_1	203.0	P_5	252.7	P_6	424.3
B_2	87.7	B_7	14.5	B_9	339.7
P_2	303.7				
B_3	318.2				
P_3	387.4				
B_4	395.7				
P_4	399.6				
B_5	321.8				

IV. SUMMARY AND OUTLOOK

In this paper, we propose and demonstrate BATIS, a fully autonomous procedure for bootstrapping, automated testing, and characterization of accumulation mode undoped QD devices. The prior knowledge about the QD device required to initialize BATIS is limited to the heterostructure, the device geometry, the ohmic biases, and the device limits. BATIS navigates through complex high-dimensional gate space to find the final gate configuration in which all desirable current channels are formed following simple physical principles.

The goal of BATIS is to test the device's functionality to confirm that all gates can properly pinch-off and that all current channels can be formed. Testing and characterizing an unknown QD device is essential for identifying global device states that are suitable for observing the Coulomb blockade. Importantly, the single-button-press testing and initialization process is demonstrated at 1.3 K, eliminating the need for a full cooldown just to learn that a device is not functional. This result is particularly important as we envision a hot large-scale spin-based quantum processor. These systems will require qubit initialization, relying on a complete and accurate device characterization. One could imagine using BATIS to probe the attributes of many devices spread across a wafer or provide device diagnostics on a portion of a large qubit processor without going to mK temperatures.

The flexible structure of BATIS allows for scalable characterization and initialization of any accumulation-mode linear array of QDs. It is also easily adaptable to other QD platforms. In particular, BATIS could straightforwardly mimic the behavior of algorithms proposed for nanowires and GaAs/Al$_x$Ga$_{1-x}$As by simply invoking skip logic on the steps not necessary for these devices. On the other hand, it is quite unlikely that any previously proposed algorithms could be easily adapted to the Si/Si$_x$Ge$_{1-x}$ quad-QD device considered in this work.

Previous studies have demonstrated device-agnostic algorithms for certain subsets of QD device-tuning tasks, such as setting QD topologies [17, 33] or charge-state classifications [24, 34]. However, these algorithms presuppose that device characterization and foundational tuning steps—such as determining gate functionality, defining the QD channel(s), or locating regions of interest for the coarse-tuning regime—have already been performed. BATIS fills this gap, bringing device characterization easily within reach for linear QD arrays and paving the way toward fully automatic control. When linked together, the proposed subroutines form an autonomous system for controlling arbitrary QD devices up to any desired level of characterization, putting QD qubit systems on the path to scalable quantum computing.

ACKNOWLEDGMENTS

We acknowledge Danielle Middlebrooks for helping with the automation. We acknowledge HRL Laboratories, LLC for support and L.F. Edge for providing one of the Si/Si$_x$Ge$_{1-x}$ heterostructures used in this work. This work was supported in part by ARO grant nos. W911NF-17-1-0274, W911NF-23-1-0110, and W911NF-24-2-0043. The authors gratefully acknowledge the use of facilities and instrumentation in the UW-Madison Wisconsin Center for Nanoscale Technology, which is partially supported by the Wisconsin Materials Research Science and Engineering Center (NSF DMR-2309000) and the University of Wisconsin-Madison. The views and conclusions contained in this paper are those of the authors and should not be interpreted as representing the official policies, either expressed or implied, of the U.S. Government. The U.S. Government is authorized to reproduce and distribute reprints for Government purposes notwithstanding any copyright noted herein. Any mention of commercial products is for information only; it does not imply recommendation or endorsement by NIST.

[1] G. Burkard, T. D. Ladd, A. Pan, J. M. Nichol, and J. R. Petta, Semiconductor spin qubits, Reviews of Modern Physics **95**, 025003 (2023).

[2] W. G. van der Wiel, S. De Franceschi, J. M. Elzerman, T. Fujisawa, S. Tarucha, and L. P. Kouwenhoven, Electron transport through double quantum dots, Rev. Mod. Phys. **75**, 1 (2002).

[3] D. Loss and D. P. DiVincenzo, Quantum computation with quantum dots, Phys. Rev. A **57**, 120 (1998).

[4] R. Hanson, L. P. Kouwenhoven, J. R. Petta, S. Tarucha, and L. M. K. Vandersypen, Spins in few-electron quantum dots, Rev. Mod. Phys. **79**, 1217 (2007).

[5] F. A. Zwanenburg, A. S. Dzurak, A. Morello, M. Y. Simmons, L. C. L. Hollenberg, G. Klimeck, S. Rogge, S. N. Coppersmith, and M. A. Eriksson, Silicon quantum electronics, Rev. Mod. Phys. **85**, 961 (2013).

[6] W. Ha, S. D. Ha, M. D. Choi, Y. Tang, A. E. Schmitz, M. P. Levendorf, K. Lee, J. M. Chappell, T. S. Adams, D. R. Hulbert, *et. al*, A flexible design platform for si/sige exchange-only qubits with low disorder, Nano Lett. **22**, 1443 (2022), pMID: 34806894.

[7] C.-A. Wang, V. John, H. Tidjani, C. X. Yu, A. S. Ivlev, C. Déprez, F. van Riggelen-Doelman, B. D. Woods, N. W. Hendrickx, W. I. L. Lawrie, *et. al*, Operating semiconductor quantum processors with hopping spins, Science **385**, 447 (2024).

[8] H. C. George, M. T. Mądzik, E. M. Henry, A. J. Wagner, M. M. Islam, F. Borjans, E. J. Connors, J. Corrigan, M. Curry, M. K. Harper, *et. al*, 12-spin-qubit arrays fabricated on a 300 mm semiconductor manufacturing line (2024), arXiv:2410.16583 [cond-mat.mes-hall].

[9] For a given current curve, the pinch-off and the turn-on voltage are mathematically indistinguishable. However, when measuring a physical gate, a hysteresis (i.e., a shift

of the current curve that depends on the direction of the sweep) can be observed.

[10] F. Borsoi, N. W. Hendrickx, V. John, M. Meyer, S. Motz, F. Van Riggelen, A. Sammak, S. L. De Snoo, G. Scappucci, and M. Veldhorst, Shared control of a 16 semiconductor quantum dot crossbar array, Nature Nanotechnology **19**, 21 (2024).

[11] S. Park, J. Benson, J. Corrigan, J. P. Dodson, S. N. Coppersmith, M. Friesen, and M. A. Eriksson, Single-shot latched readout of a quantum dot qubit using barrier gate pulsing (2024), arXiv:2408.15380 [cond-mat].

[12] L. M. K. Vandersypen, H. Bluhm, J. S. Clarke, A. S. Dzurak, R. Ishihara, A. Morello, D. J. Reilly, L. R. Schreiber, and M. Veldhorst, Interfacing spin qubits in quantum dots and donors—hot, dense, and coherent, npj Quantum Inf. **3**, 34 (2017).

[13] U. Meirav, M. A. Kastner, and S. J. Wind, Single-electron charging and periodic conductance resonances in gaas nanostructures, Phys. Rev. Lett. **65**, 771 (1990).

[14] M. de Kruijf, S. Geyer, T. Berger, M. Mergenthaler, F. Braakman, R. J. Warburton, and A. V. Kuhlmann, A compact and versatile cryogenic probe station for quantum device testing, Review of Scientific Instruments **94**, 054707 (2023).

[15] S. Neyens, O. K. Zietz, T. F. Watson, F. Luthi, A. Nethwewala, H. C. George, E. Henry, M. Islam, A. J. Wagner, F. Borjans, *et. al*, Probing single electrons across 300-mm spin qubit wafers, Nature **629**, 80 (2024).

[16] J. Darulová, S. J. Pauka, N. Wiebe, K. W. Chan, G. C. Gardener, M. J. Manfra, M. C. Cassidy, and M. Troyer, Autonomous tuning and charge-state detection of gate-defined quantum dots, Phys. Rev. Appl. **13**, 054005 (2020).

[17] A. Zubchenko, D. Middlebrooks, T. Rasmussen, L. Lausen, F. Kuemmeth, A. Chatterjee, and J. P. Zwolak, Autonomous bootstrapping of quantum dot devices, arXiv:2407.20061 (2024).

[18] T. A. Baart, P. T. Eendebak, C. Reichl, W. Wegscheider, and L. M. K. Vandersypen, Computer-automated tuning of semiconductor double quantum dots into the single-electron regime, Appl. Phys. Lett. **108**, 213104 (2016).

[19] M. Lapointe-Major, O. Germain, J. Camirand Lemyre, D. Lachance-Quirion, S. Rochette, F. Camirand Lemyre, and M. Pioro-Ladrière, Algorithm for automated tuning of a quantum dot into the single-electron regime, Phys. Rev. B **102**, 085301 (2020).

[20] B. Severin, D. T. Lennon, L. C. Camenzind, F. Vigneau, F. Fedele, D. Jirovec, A. Ballabio, D. Chrastina, G. Isella, M. De Kruijf, *et. al*, Cross-architecture tuning of silicon and SiGe-based quantum devices using machine learning, Sci. Rep. **14**, 17281 (2024).

[21] M. A. Wolfe, B. X. Coe, J. S. Edwards, T. J. Kovach, T. McJunkin, B. Harpt, D. Savage, M. G. Lagally, R. McDermott, M. Friesen, *et. al*, Control of threshold voltages in $Si/Si_{0.7}$ $Ge_{0.3}$ quantum devices via optical illumination, Physical Review Applied **22**, 034044 (2024).

[22] J. P. Zwolak, T. McJunkin, S. S. Kalantre, J. Dodson, E. R. MacQuarrie, D. Savage, M. Lagally, S. Coppersmith, M. A. Eriksson, and J. M. Taylor, Autotuning of double-dot devices in situ with machine learning, Phys. Rev. Appl. **13**, 034075 (2020).

[23] J. P. Zwolak, T. McJunkin, S. S. Kalantre, S. F. Neyens, E. R. MacQuarrie, M. A. Eriksson, and J. M. Taylor, Ray-based framework for state identification in quantum dot devices, PRX Quantum **2**, 020335 (2021).

[24] J. Ziegler, F. Luthi, M. Ramsey, F. Borjans, G. Zheng, and J. P. Zwolak, Tuning arrays with rays: Physics-informed tuning of quantum dot charge states, Phys. Rev. Appl. **20**, 034067 (2023).

[25] J. Ziegler, F. Luthi, M. Ramsey, F. Borjans, G. Zheng, and J. P. Zwolak, Automated extraction of capacitive coupling for quantum dot systems, Phys. Rev. Appl. **19**, 054077 (2023).

[26] A. S. Rao, D. Buterakos, B. van Straaten, V. John, C. X. Yu, S. D. Oosterhout, L. Stehouwer, G. Scappucci, M. Veldhorst, F. Borsoi, and J. P. Zwolak, MAViS: Modular Autonomous Virtualization System for Two-Dimensional Semiconductor Quantum Dot Arrays, arXiv:2411.12516 (2024).

[27] J. P. Zwolak and J. M. Taylor, *Colloquium*: Advances in automation of quantum dot devices control, Rev. Mod. Phys. **95**, 011006 (2023).

[28] D. M. Zajac, T. M. Hazard, X. Mi, E. Nielsen, and J. R. Petta, Scalable gate architecture for a one-dimensional array of semiconductor spin qubits, Phys. Rev. Appl. **6**, 054013 (2016).

[29] J. P. Dodson, N. Holman, B. Thorgrimsson, S. F. Neyens, E. R. MacQuarrie, T. McJunkin, R. H. Foote, L. F. Edge, S. N. Coppersmith, and M. A. Eriksson, Fabrication process and failure analysis for robust quantum dots in silicon, Nanotechnology **31**, 505001 (2020).

[30] The parameter v is defined as part of the configuration file and can be adjusted if needed.

[31] T. W. McJunkin, *Heterostructure Modifications, Fabrication Improvements, and Measurements Automation of Si/SiGe Quantum Dots for Quantum Computation*, Ph.D. thesis, The University of Wisconsin-Madison, Madison, WI, USA (2021).

[32] D. Schug, T. J. Kovach, M. A. Wolfe, J. Benson, S. Park, J. P. Dodson, J. Corrigan, M. A. Eriksson, and J. P. Zwolak, Automation of Quantum Dot Measurement Analysis via Explainable Machine Learning (2024), version Number: 4.

[33] J. Ziegler, T. McJunkin, E. S. Joseph, S. S. Kalantre, B. Harpt, D. E. Savage, M. G. Lagally, M. A. Eriksson, J. M. Taylor, and J. P. Zwolak, Toward robust autotuning of noisy quantum dot devices, Phys. Rev. Appl. **17**, 024069 (2022).

[34] R. Durrer, B. Kratochwil, J. Koski, A. Landig, C. Reichl, W. Wegscheider, T. Ihn, and E. Greplova, Automated tuning of double quantum dots into specific charge states using neural networks, Phys. Rev. Appl. **13**, 054019 (2020).